

# Copy-number signatures and mutational processes in ovarian carcinoma

Geoff Macintyre<sup>1†</sup>, Teodora E. Goranova<sup>1†</sup>, Dirlini De Silva<sup>1</sup>, Darren Ennis<sup>2</sup>, Anna M. Piskorz<sup>1</sup>, Matthew Eldridge<sup>1</sup>, Daoud Sie<sup>3</sup>, Liz-Anne Lewsley<sup>4</sup>, Aishah Hanif<sup>4</sup>, Cheryl Wilson<sup>4</sup>, Suzanne Dowson<sup>2</sup>, Rosalind M. Glasspool<sup>5</sup>, Michelle Lockley<sup>6,7</sup>, Elly Brockbank<sup>6</sup>, Ana Montes<sup>8</sup>, Axel Walther<sup>9</sup>, Sudha Sundar<sup>10</sup>, Richard Edmondson<sup>11</sup>, Geoff D. Hall<sup>12</sup>, Andrew Clamp<sup>13</sup>, Charlie Gourley<sup>14</sup>, Marcia Hall<sup>15</sup>, Christina Fotopoulou<sup>16</sup>, Hani Gabra<sup>16</sup>, James Paul<sup>4</sup>, Anna Supernat<sup>1</sup>, David Millan<sup>17</sup>, Aoisha Hoyle<sup>17</sup>, Gareth Bryson<sup>17</sup>, Craig Nourse<sup>2</sup>, Laura Mincarelli<sup>2</sup>, Luis Navarro Sanchez<sup>2</sup>, Bauke Ylstra<sup>3</sup>, Mercedes Jimenez-Linan<sup>18</sup>, Luiza Moore<sup>18</sup>, Oliver Hofmann<sup>2</sup>, Florian Markowetz<sup>1,\*</sup>, Iain A. McNeish<sup>2,5,16,\*</sup>, James D. Brenton<sup>1,18,19,\*,#</sup>

1. Cancer Research UK Cambridge Institute, Cambridge, CB2 0RE, UK
2. Institute of Cancer Sciences, University of Glasgow, G61 1QH, UK
3. VU University Medical Centre, Amsterdam 1007 MB, The Netherlands
4. Cancer Research UK Clinical Trials Unit, Institute of Cancer Sciences, University of Glasgow, G12 0YN, UK
5. Beatson West of Scotland Cancer Centre, Glasgow, G12 0YN, UK
6. Barts Cancer Institute, London, EC1M 6BQ, UK
7. University College London Hospital, London, WC1E 6BD, UK
8. Guy's Hospital, London, SE1 9RT, UK
9. Bristol Haematology and Oncology Centre, Bristol, BS2 8ED, UK
10. City Hospital, Birmingham, B18 7QH, UK
11. St Mary's Hospital, Manchester, M13 9WL, UK
12. St James Hospital, Leeds, LS9 7TF, UK
13. The Christie Hospital, Manchester, M20 4BX, UK
14. Edinburgh Cancer Research Centre, Edinburgh, EH4 2XR, UK
15. Mount Vernon Cancer Centre, Northwood, HA6 2RN, UK
16. Imperial College, London, W12 0NN, UK
17. Queen Elizabeth University Hospital, Glasgow G51 4TF, UK
18. Addenbrooke's Hospital, Cambridge, CB2 0QQ, UK.
19. Department of Oncology, University of Cambridge, CB2 0XZ

<sup>†</sup> These authors contributed equally to this work.

\* Co-corresponding authors: Florian Markowetz ([Florian.Markowetz@cruk.cam.ac.uk](mailto:Florian.Markowetz@cruk.cam.ac.uk)), Iain McNeish ([i.mcneish@imperial.ac.uk](mailto:i.mcneish@imperial.ac.uk)), James Brenton ([James.Brenton@cruk.cam.ac.uk](mailto:James.Brenton@cruk.cam.ac.uk))

# Lead contact

## Keywords

Cancer genomics, copy-number aberration, mutational signatures, mutational processes, mutator phenotype, continuum of genomes

## Abstract

The genomic complexity of profound copy-number aberration has prevented effective molecular stratification of ovarian cancers. To decode this complexity, we derived copy-number signatures from shallow whole genome sequencing of 117 high-grade serous ovarian cancer (HGSOC) cases, which were validated on 527 independent cases. We show that HGSOC comprises a continuum of genomes shaped by multiple mutational processes that result in known patterns of genomic aberration. Copy-number signature exposures at diagnosis predict both overall survival and the probability of platinum-resistant relapse. Measuring signature exposures provides a rational framework to choose combination treatments that target multiple mutational processes.

58 The discrete mutational processes that drive copy-number change in human cancers are not  
59 readily identifiable from genome-wide sequence data. This presents a major challenge for the  
60 development of precision medicine for cancers that are strongly dominated by copy-number  
61 changes, including high-grade serous ovarian (HGSOC), esophageal, non-small-cell lung and  
62 triple negative breast cancers<sup>1</sup>. These tumors have low frequency of recurrent oncogenic  
63 mutations, few recurrent copy number alterations, and highly complex genomic profiles<sup>2</sup>.

64 HGSOCs are poor prognosis carcinomas with ubiquitous *TP53* mutation<sup>3</sup>. Despite efforts to  
65 discover new molecular subtypes and targeted therapies, overall survival has not improved over  
66 two decades<sup>4</sup>. Current genomic stratification is limited to defining homologous recombination-  
67 deficient (HRD) tumors<sup>5-7</sup> with approximately 20% HGSOC cases having a germline or somatic  
68 mutation in *BRCA1/2* with smaller contributions from mutation or epigenetic silencing of other HR  
69 genes<sup>8</sup>. Classification using gene expression predominantly reflects the tumor microenvironment  
70 and is reliable in only a subset of patients<sup>9-11</sup>. Detailed genomic analysis using whole genome  
71 sequencing has shown frequent loss of *RB1*, *NF1* and *PTEN* by gene breakage events<sup>12</sup> and  
72 enrichment of amplification associated fold-back inversions in non-HRD tumors<sup>13</sup>. However, none  
73 of these approaches has provided a broad mechanistic understanding of HGSOC, reflecting the  
74 challenges of detecting classifiers in extreme genomic complexity.

75 Recent algorithmic advances have enabled interpretation of complex genomic changes by  
76 identifying mutational signatures — genomic patterns that are the imprint of mutagenic processes  
77 accumulated over the lifetime of a cancer cell<sup>14</sup>. For example, UV exposure or mismatch repair  
78 defects induce distinct, detectable single nucleotide variant (SNV) signatures<sup>14</sup>. The clinical utility  
79 of these signatures has recently been demonstrated through a combination of structural variant  
80 (SV) and SNV signatures to improve the prediction of HRD<sup>15</sup>. Importantly, these studies show that  
81 tumor genomes are shaped by multiple mutational processes and novel computational approaches  
82 are needed to identify coexistent signatures. We hypothesized that specific features of copy-  
83 number abnormalities could represent the imprints of distinct mutational processes, and developed  
84 methods to identify signatures from copy-number features in HGSOC.

## Results

### Experimental design and data collection

We generated absolute copy number profiles from 253 primary and relapsed HGSOC samples from 132 patients in the BriTROC-1 cohort<sup>16</sup> using low-cost shallow whole-genome sequencing (sWGS; 0.1×) and targeted amplicon sequencing of *TP53* (Supplementary Figure 1). These samples formed the basis of our copy-number signature identification. A subset of 56 of these cases had deep whole-genome sequencing (dWGS) performed for mutation analysis and comparison with sWGS data. Independent data sets for validation included 112 dWGS HGSOC cases from PCAWG<sup>17</sup> and 415 HGSOC cases with SNP array and whole exome sequence from TCGA<sup>8</sup>. Supplementary Figure 1a shows the REMARK diagram for selection of BriTROC-1 patients. Supplementary Figure 1b outlines which samples were used in each analysis across the three cohorts. Clinical data for the BriTROC-1 cohort are summarized in Supplementary Table 1 and Supplementary Figure 2.

### Identification and validation of copy-number signatures

To identify copy-number (CN) signatures, we computed the genome-wide distributions of six fundamental CN features for each sample: the breakpoint count per 10MB, the copy-number of segments, the difference in CN between adjacent segments, the breakpoint count per chromosome arm, the lengths of oscillating CN segment chains and the size of segments. These features were selected as hallmarks of previously reported genomic aberrations, including breakage-fusion-bridge cycles<sup>18</sup>, chromothripsis<sup>19</sup> and tandem duplication<sup>20,21</sup>.

We applied mixture modelling to separate the copy-number feature distributions from 91 BriTROC-1 samples with high quality CN profiles into mixtures of Poisson or Gaussian distributions. This resulted in a total of 36 mixture components (Figure 1a). For each sample, the posterior probability of copy-number events arising from these components was computed and summed. These sum-of-posterior vectors were then combined to form a sample-by-component sum-of-posteriors matrix. To identify copy-number signatures, this matrix was subjected to non-negative matrix factorization (NMF)<sup>22</sup>, a method previously used for deriving SNV signatures<sup>14</sup>.

NMF identified seven CN signatures (Figure 1a), as well as their defining features and exposures in each sample. The optimal number of signatures was chosen using a consensus from 1000 initializations of the algorithm and 1000 random permutations of the data combining four model selection measures (Supplementary Figure 3). We found highly similar component weights for the signatures in the two independent cohorts (PCAWG-OV and TCGA), demonstrating the robustness of both the methodology and the copy-number features (Figure 1b,  $P < 9e-05$ , median  $r = 0.86$ ).

Supplementary Table 2), despite a significant difference in exposures to CN signatures 2, 3, 4 and 5 between the cohorts ( $P < 0.05$ , two-sided Wilcoxon rank sum test, Supplementary Figure 4).

## Linking copy-number signatures with underlying mutational processes

The majority of cases analysed exhibited multiple signature exposures suggesting that HGSOC genomes are shaped by more than one mutational process. As our signature analysis reduced this genomic complexity into its constituent components, we were able to link the individual copy-number signatures to their underlying mutational processes. To do this, we used the component weights identified by NMF to determine which pattern of global or local copy-number change defined each signature. For example, for CN signature 1, the highest weights were observed for components representing low numbers of breakpoints per 10MB, long genomic segments and two breaks occurring per chromosome arm (Figure 2a, Supplementary Figure 5). Two breaks per chromosome arm suggested that the mutational process underlying this signature might be breakage-fusion-bridge (BFB) events<sup>18</sup>.

To test this hypothesis, we correlated CN signature 1 exposures with mutation data, SNV signatures, and other measures derived from deep WGS and exome sequencing (Figure 2b-e, Supplementary Figures 6, 7, 8 and 9, Supplementary Tables 3, 4, 5, 6, 7 and 8). CN signature 1 was anti-correlated with sequencing estimates of telomere length ( $r = -0.32$ ,  $P = 0.009$ ), consistent with BFB events. In addition, CN signature 1 was positively correlated with amplification-associated fold-back inversion structural variants ( $r = 0.36$ ,  $P = 0.02$ ), which have been strongly implicated in BFB events<sup>23</sup> and have also been associated with inferior survival in HGSOC<sup>13</sup>. CN signature 1 was also enriched in cases with oncogenic RAS signaling, including *NF1* loss and mutated *KRAS* ( $p = 5 \times 10^{-6}$ , Mann-Whitney test), which has previously been shown to induce chromosomal instability as a result of aberrant G2 and mitotic checkpoint controls and missegregation<sup>24,25</sup>. Taken together, these data provide independent evidence for BFB arising as a result of oncogenic RAS signaling and telomere shortening as the underlying mechanism for CN signature 1.

We applied these approaches to the remaining signatures to identify statistically significant genomic associations using a false discovery rate  $< 0.05$  (Figure 2b-e, Figure 3, Supplementary Figures 5, 6, 7, 8 and 9, Supplementary Tables 3, 4, 5, 6, 7 and 8).

CN signature 2 showed frequent breakpoints per 10MB, single changes in copy-number (resulting in 3 copies), chains of oscillating copy-number, and was significantly correlated with tandem duplicator phenotype scores ( $r = 0.3$ ,  $P = 0.004$ ) and SNV signature 5 ( $r = 0.26$ ,  $P = 0.02$ ). In addition, this signature was enriched in patients with mutations in *CDK12* ( $P = 0.02$ , Mann-Whitney test, Supplementary Table 6), in keeping with previous studies that have demonstrated large tandem duplication in cases with inactivating *CDK12* mutations<sup>26</sup>.

CN signature 4 was characterised by high copy-number states (4-8 copies) and predominant copy-number change-points of size 2. This pattern indicates a mutational process of late whole-genome duplication (WGD)<sup>27</sup>. Significantly increased signature 4 exposure in cases with aberrant PI3K/AKT signaling provided further support for late WGD as oncogenic *PIK3CA* induces tolerance to genome doubling<sup>28</sup> ( $P=2e-22$ , Mann-Whitney test, mutation of *PIK3CA* or amplification of *AKT*, *EGFR*, *MET*, *FGFR3* and *ERBB2*). Signature 4 was also seen at higher levels in cases with mutations in Toll-like receptor signaling cascades ( $P=2e-07$ ), interleukin signaling pathways ( $P=3e-24$ ) and *CDK12* ( $P=0.0009$ ), as well as those with amplified *CCNE1* ( $P=2e-10$ ) and *MYC* ( $P=9e-12$ ). It was also significantly correlated with telomere length ( $r=0.46$ ,  $P=4e-05$ ).

CN signature 6 showed extremely high copy-number states and high copy-number change-points for small segments interspersed among larger, lower-copy segments. This suggests a mutational process resulting in focal amplification. Increased signature 6 exposure was associated with mutations across diverse pathways, including aberrant G1/S cell cycle checkpoint control (through either amplification of *CCNE1*, *CCND1*, *CDK2*, *CDK4* or *MYC*, deletion/inactivation of *RB1* or mutation in *CDK12*), Toll-like receptor signaling cascades and PI3K/AKT signaling ( $P<0.05$ ). However, as many of these statistical associations are marked by gene amplification, it is difficult to determine whether the copy number states represent causal events or are simply a consequence of focal amplification. Exposure to CN signature 6 was also positively correlated with age at diagnosis ( $r=0.31$ ,  $P=6e-12$ ) and age-related SNV signature 1<sup>14</sup> ( $r=0.43$ ,  $P=3e-06$ ).

CN signature 5 was significantly associated with predicted chromothriptic-like events using the Shatterproof algorithm<sup>29</sup> ( $r=0.44$ ,  $P=2e-03$ ). Chromothripsis is considered rare in HGSOC<sup>12,27,30</sup>. However, the key component of this signature—the presence of copy-number change points centered at 0.5 copies—suggests that the events are subclonal. This implies that chromothripsis may be an underestimated oncogenic mechanism in HGSOC that could reflect ongoing formation and rupture of micronuclei<sup>31</sup>.

CN signature 3 was characterized by an even distribution of breaks across all chromosomes, and copy number changes from diploid to single copy (LOH). CN signature 3 was significantly enriched in cases with mutations in *BRCA1* and *BRCA2*, and other HR genes including *BARD1*, *PALB2* and *ATR* ( $P=0.002$ , Mann-Whitney test). It was also correlated with the HRD-related SNV signature 3 ( $r=0.32$ ,  $P=0.002$ ) and anti-correlated with age at diagnosis and age-related SNV signature 1 ( $P<0.05$ ). CN signature 3 was also enriched in cases with loss of function mutations in *PTEN* ( $P=0.002$ , Mann-Whitney test). Taken together, these data suggest that CN signature 3 is driven by *BRCA1/2*-related HRD mechanisms.

CN signature 7, like CN signature 3, also demonstrated an even distribution of breaks across all chromosomes. By contrast with CN signature 3, single copy-number changes were observed from a tetraploid rather than a diploid state (Figure 3). Although there was correlation with the HRD-

related SNV signature 3, there was no enrichment with *BRCA1/2* mutation, suggesting alternative HRD mechanisms as potential mutational processes.

We also investigated relationships between CN signatures. *BRCA1* dysfunction and *CCNE1* amplification have been shown to be mutually exclusive in HGSOC<sup>32</sup>, and we observed that CN signature 3 (*BRCA1/2* HRD) and CN signature 6 (marked by aberrant G1/S cell cycle checkpoint control) showed mutually exclusive associations (Figure 2b-e). Loss of *BRCA1* and *BRCA2* are early driver events in HGSOC, and to investigate acquisition of additional mutational processes, we studied four BriTROC-1 cases with deleterious germline *BRCA2* mutations and confirmed somatic loss of heterozygosity at *BRCA2* (Figure 4). A diverse and variable number of CN signatures was seen in these cases, including substantial exposures to CN signature 1 (RAS signaling) in three of the four cases.

## Copy-number signatures predict overall survival

We next explored the association between individual CN signature exposures and overall survival using a combined dataset of 575 diagnostic samples with clinical outcomes. We trained a multivariate Cox proportional hazards model on 417 cases and tested this on the remaining 158 cases (Figure 5, Supplementary Table 9). CN signature exposure was significantly predictive of survival (Training:  $P=0.002$ , log-rank test; stratified by age and cohort; Test:  $P=0.05$ , C-index=0.56, 95% CI:0.50-0.62; Entire cohort:  $P=0.002$ , log-rank test; stratified by age and cohort). Across the entire cohort, poor outcome was significantly predicted by CN signature 1 ( $P=0.0008$ ) and CN signature 2 exposures ( $P=0.03$ ), whilst good outcome was significantly predicted by exposures to CN signatures 3 ( $P=0.05$ ) and 7 ( $P=0.006$ ).

Unsupervised hierarchical clustering of samples by signature exposures identified three clusters (Figure 5). Despite showing significant survival differences ( $P=0.004$ , log-rank test; stratified by age and cohort), these clusters did not provide any prognostic information in addition to that identified from the Cox proportional hazards model; cluster 2 was dominated by patients with high signature 1 exposures (poor prognosis), cluster 3 showed high signature 3 exposures (good prognosis) and cluster 1 had mixed signature exposures (Supplementary Figure 10).

## Copy-number signatures indicate relapse following chemotherapy

Using a generalised linear model, we investigated whether copy-number signatures could be used to predict outcome following chemotherapy across 36 patients from the BriTROC-1 study with paired diagnostic and relapse samples<sup>16</sup>. The model showed CN signature 1 exposures at the time of diagnosis to be significantly predictive of platinum-resistant relapse ( $P=0.02$ , z-test, Supplementary Table 10).

226 Using the same 36 sample pairs, we also investigated whether chemotherapy treatment changed  
227 CN signature exposures. No significant effects on exposures were observed following  
228 chemotherapy treatment using a linear model that accounted for signature exposure at time of  
229 diagnosis, number of lines of chemotherapy and patient age ( $P>0.05$ , F-test, Supplementary Table  
230 10). The only variable showing a significant association with exposure at relapse was signature  
231 exposure at diagnosis ( $P<0.01$ , F-test, Supplementary Table 11).



## Discussion

Copy-number signatures provide a framework that is able to rederive the major defining elements of HGSOC genomes, including defective HR<sup>8</sup>, amplification of cyclin E<sup>9</sup> and amplification-associated fold-back inversions<sup>13</sup>. In addition, the CN signatures show significant associations with known driver gene mutations in HGSOC and provide the ability to detect novel associations with gene mutations. We derived signatures using inexpensive shallow whole genome sequencing of DNA from core biopsies. These approaches are rapid and cost effective, thus providing a clear path to clinical implementation. Copy-number signatures open new avenues for clinical trial design by highlighting contributions from underlying mutational processes that depend on oncogenic RAS and PI3K/AKT signaling.

We found that almost all patients with HGSOC demonstrated a mixture of signatures indicative of combinations of mutational processes. These results suggest that early *TP53* mutation, the ubiquitous initiating event in HGSOC, may permit multiple mutational processes to co-evolve, potentially simultaneously. Although further work is needed to define the precise timing of signature exposures, early driver events such as *BRCA2* mutation still permit a diverse and variable number of CN signatures in addition to an HRD signature (Figure 4). These additional signature exposures may alter the risk of developing therapeutic resistance, particularly when only a single mutational process such as HRD is targeted.

High exposure to CN signature 3, characterised by *BRCA1/2*-related HRD, is associated with improved overall survival, confirming prior data showing that *BRCA1/2* mutation is associated with long survival in HGSOC<sup>33,34</sup>. Conversely, high exposure to signature 1, which is characterised by oncogenic RAS signaling (including *NF1*, *KRAS* and *NRAS* mutation), predicts subsequent platinum-resistant relapse and poor survival. This suggests that powerful intrinsic resistance mechanisms are present at the time of diagnosis and can be readily identified using CN signature analysis. This hypothesis is supported by the presence of exposure to CN signature 1 in germline *BRCA2*-mutated cases (Figure 4) as well as our previous work demonstrating the expansion of a resistant subclonal *NF1*-deleted population following chemotherapy treatment in HGSOC<sup>35</sup> and poor outcomes in *Nf1*-deleted murine models of HGSOC<sup>36</sup>. Our CN signature analysis of *BRCA2*-mutated cases also concurs with PCAWG/ICGC data showing that over half (9/16) of *NF1*-mutated cases also harboured mutations in *BRCA1* or *BRCA2*<sup>12</sup>. These data suggest a complex interplay between RAS signaling and HRD. Thus, RAS signaling may be an important target, especially in first line treatment, to prevent emergence of platinum-resistant disease.

We found that CN signature exposures were not significantly altered between diagnosis and disease relapse in 36 sample pairs with a median interval of 30.6 months<sup>16</sup>. This suggests that the underlying mutational processes in HGSOC are relatively stable and that genome-wide patterns of copy-number change mainly reflect historic alterations to the genome acquired during

tumorigenesis<sup>37</sup>. Relative invariant genomic changes were also observed in the ARIEL2 trial, where genome-wide loss-of-heterozygosity was used to predict HRD, and only 14.5% (17/117) cases changed LOH status between diagnosis and relapse<sup>7</sup>.

Larger association studies will be required to further refine CN signature definitions and interpretation. The application of our approach to other tumour types is likely to extend the set of signatures beyond the robust core set identified here. Basal-like breast cancers, squamous cell and small cell lung carcinoma, which all have high rates of *TP53* mutation and genomic instability<sup>2</sup>, are promising next targets. Although it is likely that the strong associations have identified the driver mutational processes for CN signatures 1 and 3, functional studies will be required to establish causal links for the remaining signatures. For example, CN signature 6 was significantly associated with multiple mutated pathways, and this association was primarily driven by amplification of target genes. As this signature represented focal amplification events, it is difficult to determine whether amplification of specific genes drives the underlying mutational process or the amplifications emerge as a consequence of strong selection of advantageous phenotypes. Our data does not provide timing information for exposures and there is the real possibility that one mutational process may well drive the emergence of other mutational processes. For example, the association between signature 6 and PI3K signalling is also shared with signature 4.

Other limitations of this work are technical: we integrated data from three sources, using three different pre-processing pipelines, and the ploidy determined by different pipelines can have a significant effect on the derived signatures. For example, high-ploidy CN signature 4 was predominantly found in the sequenced samples that underwent careful manual curation to identify whole-genome duplication events. When extending to larger sample sets, a unified processing strategy with correct ploidy determination is likely to produce improved signature definitions.

Efforts to identify discrete, clinically relevant subtypes of disease have been successful in many cancer types<sup>38-40</sup>. However, HGSOC lacks clinically-relevant patient stratification, which is reflected in continued poor survival. We show that HGSOC genomes are shaped by multiple mutational processes that preclude simple subtyping. Thus, our results suggest that HGSOC is a continuum of genomes. By dissecting the mutational forces shaping HGSOC genomes, our study paves the way to understanding extreme genomic complexity, as well as revealing the evolution of tumors as they relapse and acquire resistance to chemotherapy.

## Author contributions

Conceptualisation: GM, TEG, FM, IMcN, JDB; Study conduct: SD, RMG, ML, EB, AM, AW, SS, RE, GDH, AC, CG, MH, CF, HG, DM, AHo, GB, IMcN, JDB; Investigation: TEG, DE, AMP, LAL, AHa, CW, CN, LMi, LNS, MJL, LMo, AS, JP; Formal analysis: GM, TEG, DDS, ME, DS, BY, OH, FM; Methodology and software: GM, DDS, FM; Writing: GM, TEG, DDS, FM, IMcN, JDB

## Acknowledgements

The BriTROC-1 study was funded by Ovarian Cancer Action (to IMcN and JDB, grant number 006). We would like to acknowledge funding and support from Cancer Research UK (grant numbers A15973, A15601, A18072, A17197 and A19274), the Universities of Cambridge and Glasgow, National Institute for Health Research Cambridge and Imperial Biomedical Research Centres, National Cancer Research Network, the Experimental Cancer Medicine Centres at participating sites, the Beatson Endowment Fund and Hutchison Whampoa Limited. The funders had no role in study design, data collection and analysis, decision to publish or preparation of the manuscript. We thank the Biorepository, Bioinformatics, Histopathology and Genomics Core Facilities of the Cancer Research UK Cambridge Institute and the Pathology Core at the Cancer Research UK Beatson Institute for technical support. We would like to thank members of PCAWG Evolution and Heterogeneity Working Group for the consensus copy-number analysis, PCAWG Structural Variation Working Group for the consensus structural variants and PCAWG Technical Working Group for annotating driver mutations in the 112 PCAWG-OV samples.

## Figure Legends

### **Figure 1 | Copy-number signature identification from shallow whole genome sequence data and validation in independent cohorts**

**a.** Step 1: Absolute copy-numbers are derived from sWGS data; Step 2: genome-wide distributions of six fundamental copy-number features are computed; Step 3: Gaussian or Poisson mixture models (depending on data type) are fitted to each distribution and the optimal number of components is determined (ranging from 3–10) ; Step 4: the data are represented as a matrix with 36 mixture component counts per tumor. Step 5: Non-negative matrix factorization is applied to the components-by-tumor matrix to derive the tumor-by-signature matrix and the signature-by-components matrix.

**b.** Heat maps show component weights for copy number signatures in two independent cohorts of HGSOC samples profiled using WGS and SNP array. Correlation coefficients are provided in Supplementary Table 2.

### **Figure 2 | Linking copy-number signatures with mutational processes**

**a** Component weights for copy number signature 1. Barplots (upper panel) are grouped by copy number feature and show weights for each of the 36 components. The middle panel shows the mixture models of each distribution with components defining CN signature 1 highlighted in color. Lower panel shows genome-wide distribution (density) of each copy number feature, across the BriTROC-1 cohort, weighted by signature exposure. (Note: similar plots for other CN signatures are shown in Figure 3 and Supplementary Figure 5).

**b** Associations between CN signature exposures and other features. Purple indicates positive correlation and orange negative correlation (see also Supplementary Figure 6). Numbers at the right of the panel indicate cases included in each analysis. Only significant correlations are shown ( $P < 0.05$ ).

**c** Associations between CN signature exposures and SNV signatures. Purple indicates positive correlation and orange negative correlation (see also Supplementary Figure 6). The number at the right of the panel indicates cases included in the analysis.

**d and e** Difference in CN signature exposures between cases with mutations in specific genes (**d**) and mutated/wildtype reactome pathways (**e**). The absolute difference in mean signature exposures was calculated for cases with and without mutations. Colors in filled circles indicate extent of difference. Only differences with FDR  $P < 0.05$  (Mann-Whitney test) are shown (see also Supplementary Figure 7).

Numbers at the right of the panel indicate cases with mutations (SNVs, amplifications or deletions) in each gene/pathway.

**Figure 3 | The seven copy-number signatures in HGSOC**

Description of the defining component weights, key associations and proposed mechanisms for the seven copy number signatures.

\*only the top three mutated genes for each of the pathways associated with CN signatures 4, 6 and 7 are shown (the list of all significant genes is provided in Supplementary Tables 7 and 8).

**Figure 4 | CN signature exposures of four BriTROC-1 patients with germline *BRCA2* mutations and somatic loss of heterozygosity**

Stacked bar plots show copy-number signature exposures for four BriTROC-1 cases with pathogenic germline *BRCA2* mutations and confirmed somatic loss of heterozygosity (LOH) at the *BRCA2* locus.

**Figure 5 | Association of survival with copy-number signatures**

Upper panel: Stacked barplots show CN signature exposures for each patient. Patients were ranked by risk of death estimated by a multivariate Cox proportional hazards model stratified by age and cohort, with CN signature exposures as covariates.

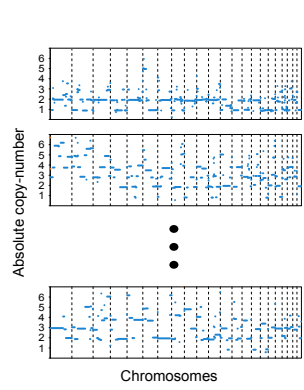
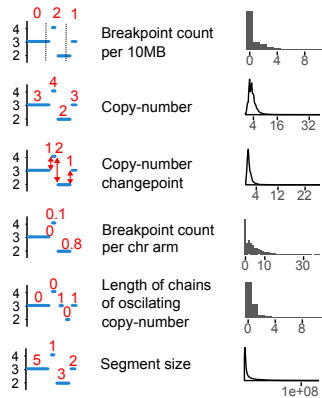
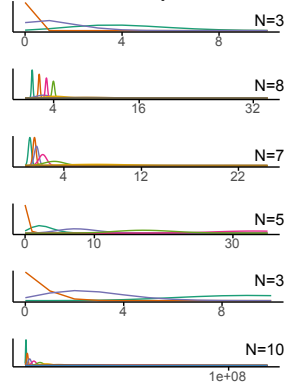
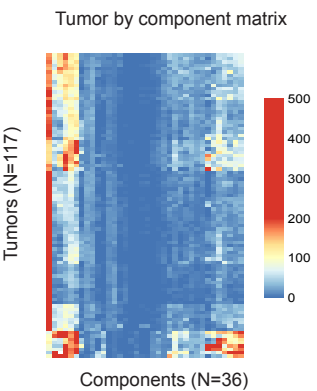
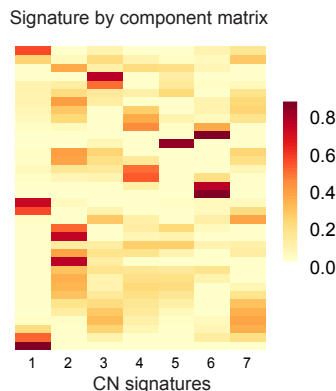
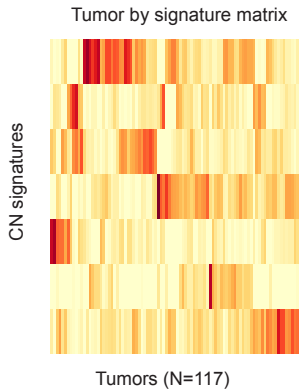
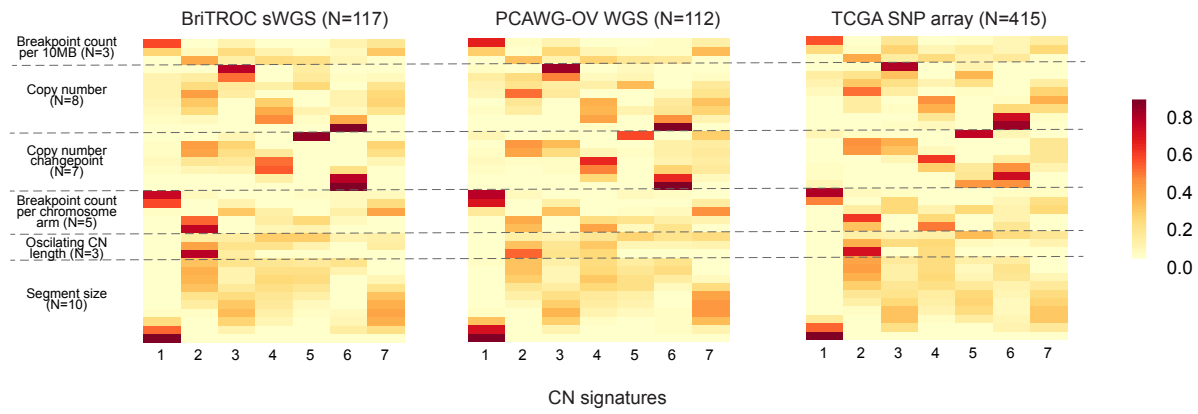
Middle panel: Colored matrix indicates group for each patient assigned by unsupervised clustering of CN signature 1, 2, 3 and 7 exposures (see also Supplementary Figure 10).

Lower panel: Linear fit of signature exposures ordered by risk predicted by the Cox proportional hazards model.

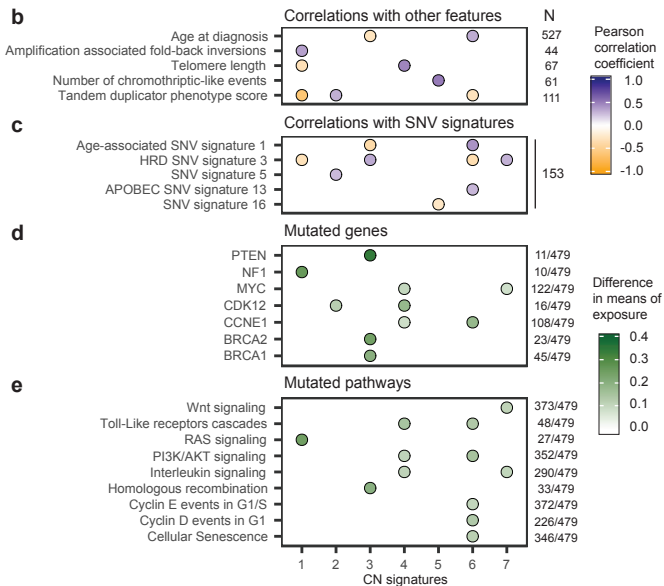
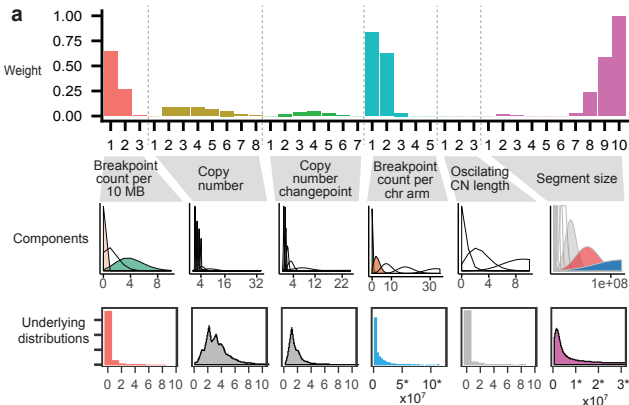
## 389 References

- 390 1. Ciriello, G. *et al.* Emerging landscape of oncogenic signatures across human cancers. *Nat*  
391 *Genet* **45**, 1127-33 (2013).
- 392 2. Hoadley, K.A. *et al.* Multiplatform analysis of 12 cancer types reveals molecular  
393 classification within and across tissues of origin. *Cell* **158**, 929-44 (2014).
- 394 3. Ahmed, A.A. *et al.* Driver mutations in TP53 are ubiquitous in high grade serous carcinoma  
395 of the ovary. *J Pathol* **221**, 49-56 (2010).
- 396 4. Vaughan, S. *et al.* Rethinking ovarian cancer: recommendations for improving outcomes.  
397 *Nat. Rev. Cancer* **11**, 719-725 (2011).
- 398 5. Fong, P.C. *et al.* Poly(ADP)-Ribose Polymerase Inhibition: Frequent Durable Responses in  
399 BRCA Carrier Ovarian Cancer Correlating With Platinum-Free Interval. *J. Clin. Oncol.* **28**,  
400 2512-2519 (2010).
- 401 6. Gelmon, K.A. *et al.* Olaparib in patients with recurrent high-grade serous or poorly  
402 differentiated ovarian carcinoma or triple-negative breast cancer: a phase 2, multicentre,  
403 open-label, non-randomised study. *Lancet Oncol.* **12**, 852-861 (2011).
- 404 7. Swisher, E.M. *et al.* Rucaparib in relapsed, platinum-sensitive high-grade ovarian  
405 carcinoma (ARIEL2 Part 1): an international, multicentre, open-label, phase 2 trial. *Lancet*  
406 *Oncol* **18**, 75-87 (2017).
- 407 8. TCGA. Integrated genomic analyses of ovarian carcinoma. *Nature* **474**, 609-615 (2011).
- 408 9. Etemadmoghadam, D. *et al.* Integrated genome-wide DNA copy number and expression  
409 analysis identifies distinct mechanisms of primary chemoresistance in ovarian carcinomas.  
410 *Clin. Cancer Res.* **15**, 1417-1427 (2009).
- 411 10. Verhaak, R.G. *et al.* Prognostically relevant gene signatures of high-grade serous ovarian  
412 carcinoma. *J Clin Invest* **123**, 517-25 (2013).
- 413 11. Chen, G.M. *et al.* Consensus on Molecular Subtypes of Ovarian Cancer. *bioRxiv* (2017).
- 414 12. Patch, A.-M. *et al.* Whole-genome characterization of chemoresistant ovarian cancer.  
415 *Nature* **521**, 489-494 (2015).
- 416 13. Wang, Y.K. *et al.* Genomic consequences of aberrant DNA repair mechanisms stratify  
417 ovarian cancer histotypes. *Nat Genet* **49**, 856-865 (2017).
- 418 14. Alexandrov, L.B. *et al.* Signatures of mutational processes in human cancer. *Nature* **500**,  
419 415-21 (2013).
- 420 15. Nik-Zainal, S. *et al.* Landscape of somatic mutations in 560 breast cancer whole-genome  
421 sequences. *Nature* **534**, 47-54 (2016).
- 422 16. Goranova, T. *et al.* Safety and utility of image-guided research biopsies in relapsed high-  
423 grade serous ovarian carcinoma-experience of the BriTROC consortium. *Br J Cancer* **116**,  
424 1294-1301 (2017).
- 425 17. Campbell, P.J. *et al.* Pan-cancer analysis of whole genomes. in *bioRxiv* (2017).
- 426 18. Murnane, J.P. Telomere dysfunction and chromosome instability. *Mutat Res* **730**, 28-36  
427 (2012).
- 428 19. Korbel, J.O. & Campbell, P.J. Criteria for inference of chromothripsis in cancer genomes.  
429 *Cell* **152**, 1226-36 (2013).
- 430 20. Ng, C.K. *et al.* The role of tandem duplicator phenotype in tumour evolution in high-grade  
431 serous ovarian cancer. *J Pathol* **226**, 703-12 (2012).
- 432 21. Menghi, F. *et al.* The tandem duplicator phenotype as a distinct genomic configuration in  
433 cancer. *Proc Natl Acad Sci U S A* **113**, E2373-82 (2016).
- 434 22. Lee, M. *et al.* Comparative analysis of whole genome sequencing-based telomere length  
435 measurement techniques. *Methods* **114**, 4-15 (2017).
- 436 23. Zakov, S., Kinsella, M. & Bafna, V. An algorithmic approach for breakage-fusion-bridge  
437 detection in tumor genomes. *Proc Natl Acad Sci U S A* **110**, 5546-51 (2013).
- 438 24. Knauf, J.A. *et al.* Oncogenic RAS induces accelerated transition through G2/M and  
439 promotes defects in the G2 DNA damage and mitotic spindle checkpoints. *J Biol Chem*  
440 **281**, 3800-9 (2006).
- 441 25. Saavedra, H.I., Fukasawa, K., Conn, C.W. & Stambrook, P.J. MAPK mediates RAS-  
442 induced chromosome instability. *J Biol Chem* **274**, 38083-90 (1999).

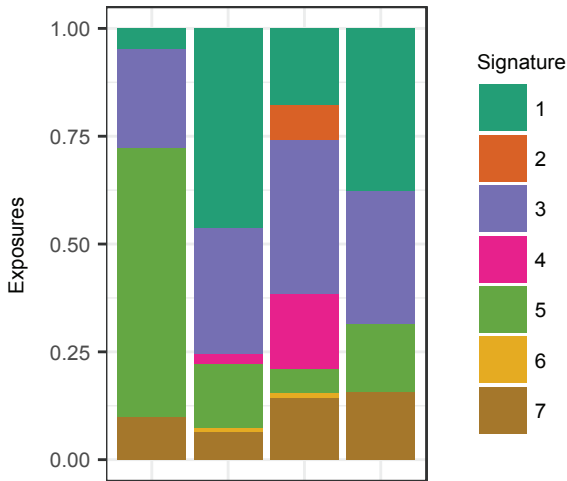
- 443 26. Popova, T. *et al.* Ovarian Cancers Harboring Inactivating Mutations in CDK12 Display a  
444 Distinct Genomic Instability Pattern Characterized by Large Tandem Duplications. *Cancer*  
445 *Res* **76**, 1882-91 (2016).
- 446 27. Zack, T.I. *et al.* Pan-cancer patterns of somatic copy number alteration. *Nat Genet* **45**,  
447 1134-40 (2013).
- 448 28. Berenjeno, I.M. *et al.* Oncogenic PIK3CA induces centrosome amplification and tolerance  
449 to genome doubling. *Nat Commun* **8**, 1773 (2017).
- 450 29. Govind, S.K. *et al.* ShatterProof: operational detection and quantification of chromothripsis.  
451 *BMC Bioinformatics* **15**, 78 (2014).
- 452 30. Malhotra, A. *et al.* Breakpoint profiling of 64 cancer genomes reveals numerous complex  
453 rearrangements spawned by homology-independent mechanisms. *Genome Res* **23**, 762-  
454 76 (2013).
- 455 31. Bakhoun, S.F. *et al.* Chromosomal instability drives metastasis through a cytosolic DNA  
456 response. *Nature* **553**, 467-472 (2018).
- 457 32. Etemadmoghadam, D. *et al.* Synthetic lethality between CCNE1 amplification and loss of  
458 BRCA1. *Proc Natl Acad Sci U S A* **110**, 19489-94 (2013).
- 459 33. Candido Dos Reis, F.J. *et al.* Germline mutation in BRCA1 or BRCA2 and ten-year survival  
460 for women diagnosed with epithelial ovarian cancer. *Clin Cancer Res* **21**, 652-7 (2015).
- 461 34. Norquist, B.M. *et al.* Mutations in Homologous Recombination Genes and Outcomes in  
462 Ovarian Carcinoma Patients in GOG 218: An NRG Oncology/Gynecologic Oncology Group  
463 Study. *Clin Cancer Res* **24**, 777-783 (2018).
- 464 35. Schwarz, R.F. *et al.* Spatial and temporal heterogeneity in high-grade serous ovarian  
465 cancer: a phylogenetic analysis. *PLoS Med* **12**, e1001789 (2015).
- 466 36. Walton, J.B. *et al.* CRISPR/Cas9-derived models of ovarian high grade serous carcinoma  
467 targeting Brca1, Pten and Nf1, and correlation with platinum sensitivity. *Scientific Reports*  
468 **7**, 16827 (2017).
- 469 37. Gerstung, M. *et al.* The evolutionary history of 2,658 cancers. *bioRxiv* (2017).
- 470 38. Curtis, C. *et al.* The genomic and transcriptomic architecture of 2,000 breast tumours  
471 reveals novel subgroups. *Nature* **486**, 346-52 (2012).
- 472 39. Kandoth, C. *et al.* Integrated genomic characterization of endometrial carcinoma. *Nature*  
473 **497**, 67-73 (2013).
- 474 40. Secrier, M. *et al.* Mutational signatures in esophageal adenocarcinoma define etiologically  
475 distinct subgroups with therapeutic relevance. *Nat Genet* **48**, 1131-41 (2016).
- 476

**a****Compute absolute CN from shallow WGS****Derive CN feature distributions****Fit optimal number of mixture model components****Compile sum-of-posteriors matrix****Perform non-negative matrix factorisation****b**





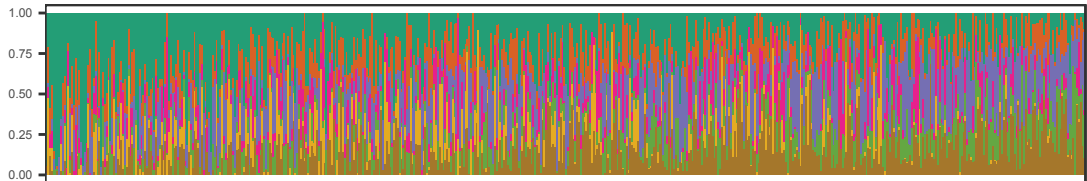
CN signature component weights	Important components	Key associations	Proposed mechanism
<p><b>Signature 1</b></p>	<p>A. Low number of breakpoints (&lt;1break/10Mb)  B. 0 or 2 breakpoints per chromosome arm  C. Large segment sizes (&gt;30Mb)</p>	<ul style="list-style-type: none"> <li>• <b>Poor overall survival</b></li> <li>• Higher in cases with mutated NF1 and RAS signaling pathway: <i>NF1, KRAS, RASA1, RASA2, CUL3, NRAS</i></li> <li>• Correlated with amplification associated fold-back inversions</li> <li>• Anti-correlated with telomere length; tandem-duplicator phenotype score; HRD SNV signature 3</li> </ul>	Oncogenic RAS/MAPK signaling and telomere shortening leading to breakage-fusion-bridge events
<p><b>Signature 2</b></p>	<p>A. High number of breakpoints (~4/10Mb)  B. Single copy-number changes resulting in 3 copies  C. Long chains of oscillating copy-number  D. Small segment size (mostly 0.4-4.3Mb)</p>	<ul style="list-style-type: none"> <li>• <b>Poor overall survival</b></li> <li>• Correlated with tandem duplicator score; SNV signature 5</li> <li>• Higher in cases with CDK12 mutation</li> </ul>	Tandem duplication through CDK12 inactivation
<p><b>Signature 3</b></p>	<p>A. Copy-number changes from diploid to single copy  B. Breaks distributed evenly across genome</p>	<ul style="list-style-type: none"> <li>• <b>Good overall survival</b></li> <li>• Higher in cases with mutation in <i>BRCA1, BRCA2, PTEN</i> and the homologous recombination pathway: <i>BARD1, PALB2, BRCA1, ATR, BLM, ATM, NBN, MRE11, BRCA2</i></li> <li>• Correlated with HRD SNV signature 3</li> <li>• Anti-correlated with age at diagnosis; age-related SNV signature 1</li> </ul>	BRCA1/2 related homologous recombination deficiency
<p><b>Signature 4</b></p>	<p>A. High segment copy-number (4-8 copies)  B. Copy-number changes of 2-3 copies</p>	<ul style="list-style-type: none"> <li>• Higher in cases with mutated MYC, CDK12, CCNE1 and mutations in the PI3K/AKT signaling, TLR cascade and interleukin signaling pathways*: <i>AKT2, RICTOR, MET, JUN, MAP2K4, PPP2R1A, MYC, SOX2, JAK2</i></li> <li>• Correlated with telomere length</li> </ul>	Whole genome duplication due to failure of cell cycle control and PI3K inactivation
<p><b>Signature 5</b></p>	<p>A. Subclonal copy-number changes (~0.5 copies)</p>	<ul style="list-style-type: none"> <li>• Correlated with number of chromothriptic-like events</li> <li>• Anti-correlated with SNV signature 16</li> </ul>	Subclonal cataphoric chromothriptic-like events through unknown mechanisms
<p><b>Signature 6</b></p>	<p>A. Large copy-number changes (6-28) resulting in high copy-number states (8-30 copies)  B. Short segments interspersed with long segments</p>	<ul style="list-style-type: none"> <li>• Higher in cases with mutated <i>CCNE1</i>, and mutations in the TLR cascade, PI3K/AKT signaling, CCNE1- and CCND1-associated events and cellular senescence pathways*: <i>AKT2, RICTOR, MET, JUN, MAP2K4, PPP2R1A, MYC, CCNE1, CCND2, CCND3, CDK6, MDM4</i></li> <li>• Correlated with age at diagnosis; age-related SNV signature 1; APOBEC SNV signature 13</li> <li>• Anti-correlated with tandem duplicator score; HRD-associated SNV signature 3</li> </ul>	Focal amplification due to failure of cell cycle control
<p><b>Signature 7</b></p>	<p>A. Copy-number changes from tetraploid to 3 copies  B. Breaks distributed evenly across genome</p>	<ul style="list-style-type: none"> <li>• <b>Good overall survival</b></li> <li>• Higher in cases with mutated MYC and mutations in the Wnt signaling and interleukin signaling pathways*: <i>MYC, SOX2, TERT, AKT2, JAK2</i></li> <li>• Correlated with HRD-associated SNV signature 3</li> </ul>	Non-BRCA1/2 related homologous recombination deficiency



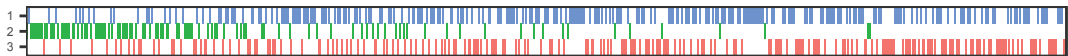
BRCA2 germline mutation carriers + somatic LOH (n=4)

Risk of death

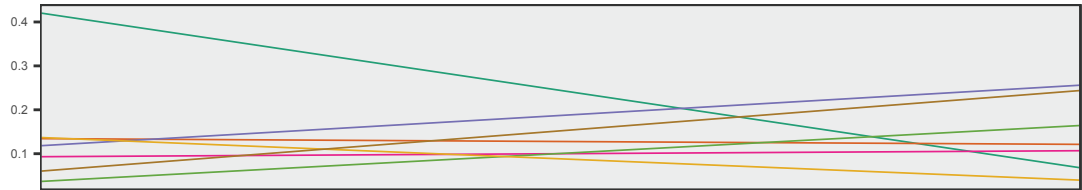
Stacked signature exposures



Unsupervised clustering



Smoothed signature exposures



Tumors ordered by decreasing risk of death (n=575)

CN  
signature

